Electronic Supplementary Material (ESI) for Materials Chemistry Frontiers.

Supporting information:

Ultrathin Nanoplatelets of Six-Line Ferrihydrite Enhances the Magnetic Properties of Hexaferrite

Harikrishnan Vijayan, Cecilie Grønvaldt Knudsen, Mathias Ibsen Mørch, Mogens Christensen*

Department of Chemistry and Interdisciplinary Nanoscience Center (iNANO), Aarhus University, Langelandsgade 140, 8000 Aarhus C, Denmark

Correspondence to: mch@chem.au.dk

Experimental Section:

Figure S1 gives an overview of the temperature and pressure used in the spark plasma sintering compaction.

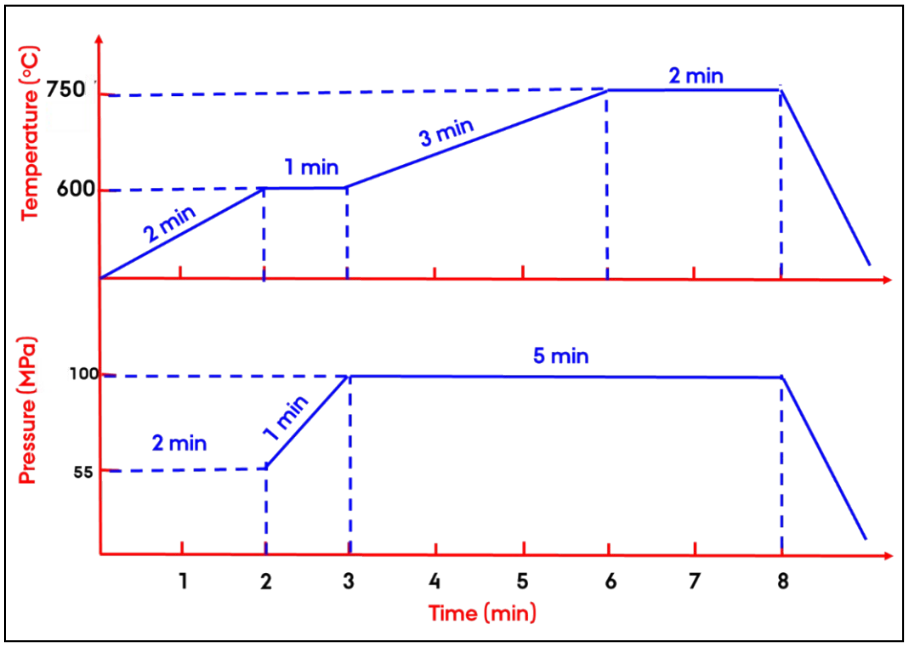

Fig. S1 SPS program used for sintering the Six-Line Ferrihydrite (SLF-100, SLF-150, SLF-200) nanoparticles leading to the conversion of $SrFe_{12}O_{19}$ along with alignment taking place during the sintering process

Transmission Pole figure measurement

Figure S2 showing the geometry of set up for Transmission pole figure analysis.

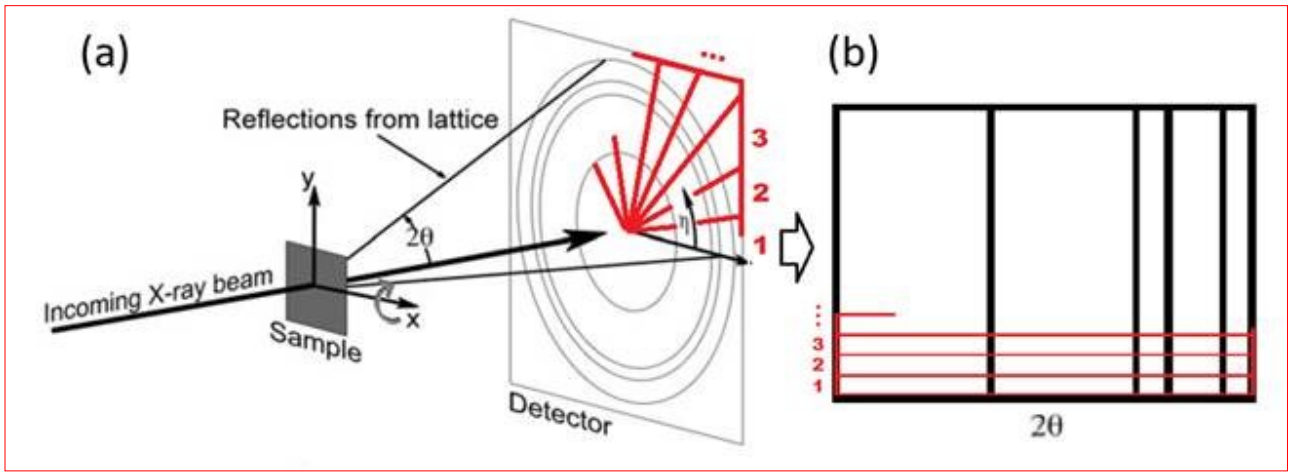

Fig. S2 (a) Represents the geometry of the set up for transmission pole figure analysis with (b) caking marked 1, 2 , 3 etc with 72 total slices.

Discussion on the structure of Six-line Ferrihydrite

The ambiguity in understanding the Six-Line Ferrihydrite phase has continued over the years. Ferrihydrite is a form of iron oxyhydroxides, which is considered an important phase in iron cycle and is found in places where iron has rapidly precipitated out of solution[1,2]. The Six-Line phase obtained from the hydrothermal synthesis in this particular study was refined based on based on the Dritts Model [3] and was well elucidated by Jansen et al. [4]. This particular model explains the structure of Six-Line Ferrihydrite as two variants namely defective phase (d) and defective free phase (f). The f-phase (*P*-31*c*) consists of the anionic ABACA closed packing in which the Fe atoms occupy only the octahedral sites. The d-phase, which consists of a subunit of the f-phase originates from a symmetry reduction (*P*-31*c* to *P*3) which involves atomic site splitting's and consequently a higher degree of disorder due to varying occupancies. The early structure of Six-line Ferrihydrite had been proposed by Dritts et al., 1993, describing the structure consisting of octahedral coordination of Fe without the presence of tetrahedral coordination of Fe [3]. The 'Dritts model' is described as multiphasic model derived from powder diffraction data. This model comprises three important phase namely the defect free phase (f-phase) ($FeO_{0.85}OH$), defective phase (d-phase) and nanocrystalline hematite (α-Fe_2O_3) phase. The Fe atoms are considered to occupy 50% of the octahedral site in f-phase while d-phase is considered to be disordered feroxyhite (δ-FeOOH). The defect free phase (f-phase) and defective phase (d-phase) have been described with hexagonal space group with *P*-31*c* and *P*3 respectively. The lattice constant proposed for this model was reported to be a = b = 2.955 Å and c = 9.37 Å. Another model for the Six-line Ferrihydrite which was widely accepted was proposed by Michel et al., [5]. This single model considered the presence of both tetrahedral and octahedral coordination of Fe in the structure with 20% and 80% occupation unlike Dritts Model. Three structures based on different coherent scattering domains (CSD) of 2, 3 and 6 nm were proposed in this model. The analysis was carried out by pair distribution function (PDF) thus employing real space for the analysis of structure. Since then there has been strong debate going on in order to define the structure of this controversial Six-Line Ferrihydrite [1,6–10]. Analyzing the structure based on pair distribution function (PDF) is beyond the scope of this work. Numerous reports are available where Ferrihydrite (Two-line and Six-line Ferrihydrite) acts as a precursor to form Goethite (α-FeOOH) and hematite (α-Fe_2O_3) nanoparticles [9,11–17].

Transmission Electron Microscopy (TEM)

Goethite impurity in SLF-200 sample is seen in Figure S3, the crystallite clearly forms small needles.

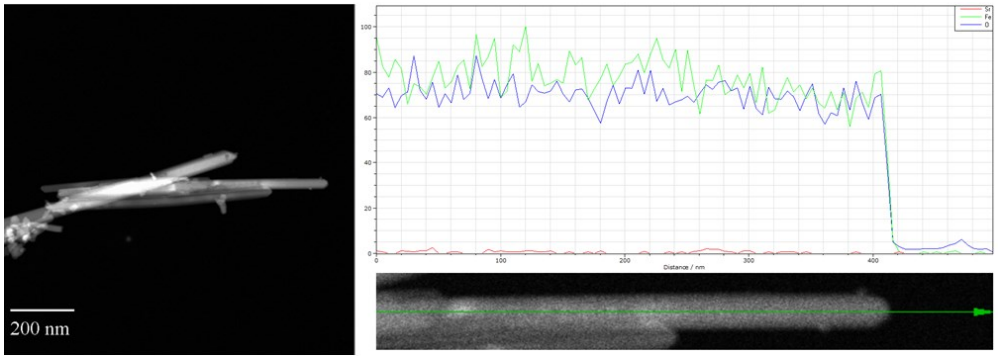

Fig. S3 Line scan was performed on the needle from the STEM arrangement. The elemental analysis drawn from the line scan showed the presence of Fe and O elements further confirming the presence of α-FeOOH (Goethite) in the needle-shaped structures from the STEM-HAADF micrographs.

Annealing of the SPS pellets

Post-annealing of the SPS pellets were carried out. Three pieces of dimensions ~ 2x2x1 mm^3 were cut out from each of the three pellets SPS-100, SPS-150 and SPS-200 and annealed at 850 °C for 2, 4 and 8 hours, respectively. Hysteresis curves of SPS-100, SPS-150 and SPS-200 annealed at 0, 2, 4 and 8 h are given in **Fig. S4 (a)-(c)**. The numeric values of M_r/M_s, H_C, and $(BH)_{max}$ are given in **table 1**.

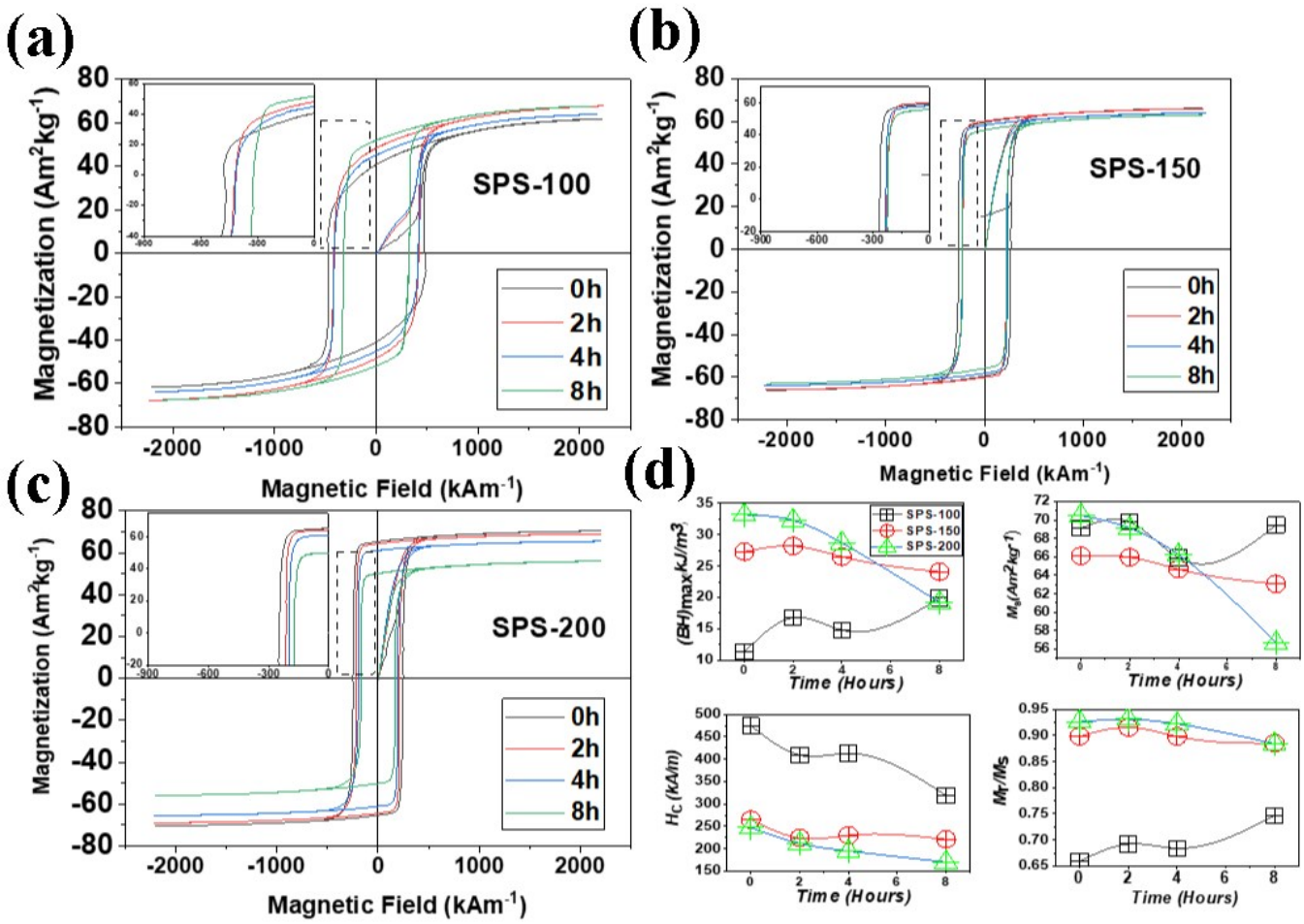

Fig. S4(a) (b) (c) The hysteresis loops of the SPS pellet samples annealed at 850 °C for 0, 2, 4 and 8 h for the SPS-100, SPS-150, SPS-200 pellets (d) Represents plot with variation of *(BH)*max, M_s, H_C, M_r/M_s with annealing temperature of 0,2,4, and 8 h.

The three SPS pellets with T_{Hyd} of 100, 150 and 200 °C behaved differently with the SPS pellets were annealed for 2, 4 and 8 h. Post annealed SPS-1 pellets (T_{Hyd} = 100°C) **(Fig. S4(a))** showed a remarkable improvement M_r/M_s value of 0.748 and M_s = 69.45(3) Am^2kg^{-1} was obtained after 8 h of annealed. This corresponds to an improvement of the $(BH)_{max}$ going from 11(4) kJ/m^3 to 19(2) kJ/m^3 after annealing alas the improvement reduces the coercivity from 474(3) to 319(4) kAm^{-1}. The decrease in H_C is attributed to the improvement alignment along the *c*-axis or growth of the crystallites into the multidomain size range. Post annealed SPS-150 (T_{Hyd} = 150°C) **(Fig. S4(b))** pellets behaved differently from the SPS-100 counterparts. The M_s and H_C reduces slightly, while rectangularity is almost constant. The $(BH)_{max}$ of those post annealed SPS-150 pellets decreased marginally from

27(4) to 24(3) kJ/m^3. There was a drastic change in the magnetic properties of post annealed SPS-3 (T_{Hyd} = 200 °C) pellets **(Fig. S4(c)).** The variation of magnetic properties such as M_s, H_C & (M_r/M_s) with annealing time has been graphically depicted in **Fig. S4 (d)**. The M_s and H_C of the post-annealed samples decreased from 71.24(2) to 56.69(2) Am^{2}kg^{-1} and 247(5) to 170(4) kJ/m^3. The drastic decrease in M_s values points to structural changes taking place in the sample, however the sample size of 2x2 mm^2 is too small for PXRD to be collected reliably and understanding the change is out of scope for the present paper. The $(BH)_{max}$ of post annealed SPS-200 pellets are found to be decreasing from the highest value of 33 kJ/m^3 to the lowest of 19 kJ/m^3. This in turn shows that post-annealing of SPS-200 pellets leads to a decrease in magnetic properties and hence this method of post annealing the SPS-200 pellets is not appropriate to improve the magnetic properties as far as the aligned particles are concerned

The $(BH)_{max}$ of the post annealed samples are compared in **Fig. S4(d)**. It has been observed that post annealed SPS-100 pellet show an improvement in the $(BH)_{max}$ values post annealed at 2, 4 and 8 h. The maximum kJm^{-3} was observed during 8 h of annealing (19 kJm^{-3}). This underlines the fact that lower (T_{Hyd} =100 °C) without any annealing shows poor degree of sample alignment. It should also be noted that alignment of such pellets can be improved by the process of post annealing. On the contrary SPS-150 pellets showed only marginal decrease in the magnetic properties and $(BH)_{max}$ as well. The magnetic properties of SPS-200 pellets decreased drastically during the post annealing process for 2, 4 and 8 h. Although the rectangularity of hysteresis was not affected during the post annealing process, there was decrease in the M_s and H_C values of the pellets. The $(BH)_{max}$ of the pellets drastically reduced from 28 to 19 kJ/m^3 during 4 and 8 h of annealing. The decrease in H_C may be due to excessive grain growth taking place during the post annealing process. There is a possibility that the grains grow more than the estimated stable single domains size there by decreasing the H_C. However, contrasting results of post annealing process for SPS-100 and SPS-200 were observed in the present work and this needs to be investigated further.

Sample	t (hours)	M_r/M_s	M_s (Am^{2}kg^{-1})	H_C (kAm^{-1})	$(BH)_{max}$ (kJm^{-3})
SPS-100	0	0.66	61.91(3)	474(3)	11(4)
	2	0.69	69.79(2)	409(3)	16(2)
	4	0.69	65.89(3)	413(4)	14(2)
	8	0.75	69.45(3)	319(4)	19(2)
SPS-150	0	0.90	66.99(2)	265(3)	27(4)
	2	0.92	65.95(3)	224(4)	28(3)
	4	0.90	64.64(3)	230(3)	26(3)
	8	0.89	63.06(2)	221(3)	24(3)
SPS-200	0	0.93	71.24(2)	247(5)	33(4)
	2	0.93	69.13(3)	212(4)	32(3)
	4	0.92	66.23(3)	195(4)	28(3)
	8	0.88	56.69(2)	170(4)	19(3)

Table S1. Summary of magnetic properties of SPS pellets annealed for 0, 2, 4 and 8 h at 850^{o}C/2 hr

References

1 R. Harrington, R. B. Neder and J. B. Parise, *Chem. Geol.*, 2012, **329**, 3–9.

2 J. L. Jambor and J. E. Dutrizac, *Chem. Rev*, 1998, **98**, 2549–2585.

3 V. A. Drits, A. L. Salyn, B. A. Sakharov and A. Manceau, *Clay Miner.*, 1993, **28**, 185–207.

4 E. Jansen, A. Kyek, W. Schäfer and U. Schwertmann, *Appl. Phys. A Mater. Sci. Process.*, 2002, **74**, 1004–1006.

5 F. M. Michel, L. Ehm, S. M. Antao, P. L. Lee, P. J. Chupas, G. Liu, D. R. Strongin, M. A. A. Schoonen, B. L. Phillips and J. B. Parise, *Science (80-.).*, 2007, **316**, 1726–1729.

6 A. Manceau, S. Skanthakumar and L. Soderholm, *Am. Mineral.*, 2014, **99**, 102–108.

7 A. Manceau, *Clay Miner.*, 2009, **44**, 19–34.

8 V. Barrón, J. Tottent and F. M. Michel, *Am. Mineral.*, 2012, **97**, 253–254.

9 F. M. Michel, V. Barrón, J. Torrent, M. P. Morales, C. J. Serna, J. Boily and Q. Liu, 2010, **107**, 2787–2792.

10 A. Manceau and L. Ge, *Clay Miner.*, 2010, **45**, 225–228.

11 S. Das, M. J. I. M. Hendry and J. Essilfie-dughan, *Environ. Sci. Technol.*, 2011, **45**, 268–275.

12 D. Zhang, S. Wang, Y. Wang, M. A. Gomez, Y. Duan and Y. Jia, *ACS Earth Sp. Chem.*, 2018, 577–587.

13 Q. Liu, V. Barro, J. Tottent, S. G. Eeckhout and C. Deng, *J. Geophys. Res. Solid Earth*, 2008, **113**, 1–12.

14 V. Barrón, J. Tottent and E. de Grave, *Am. Mineral.*, 2003, **88**, 1679–1688.

15 M. Lin, L. Tng, T. Lim, M. Choo, J. Zhang, H. R. Tan and S. Bai, *J. Phys. Chem. C*, 2014, **118**, 10903–10910.

16 M. A. Blesa, *Adv. Colloid Interface Sci.*, 1989, **29**, 173–221.

17 S. P. Schwaminger, R. Surya, S. Filser, A. Wimmer, F. Weigl, P. Fraga-García and S. Berensmeier, *Sci. Rep.*, 2017, **7**, 1–9.